Journal of The Electrochemical Society, **156** (8) P132-P138 (2009)
0013-4651/2009/156(8)/P132/7/$25.00 © The Electrochemical Society

Coloration Mechanism in Proton-Intercalated Electrochromic Hydrated NiO_y and $Ni_{1-x}V_xO_y$ Thin Films

E. Avendaño,[a,c,e] H. Rensmo,[b] A. Azens,[c,d] A. Sandell,[b] G. de M. Azevedo,[e] H. Siegbahn,[b] G. A. Niklasson,[a,z] and C. G. Granqvist[a,*]

[a]*Department of Engineering Sciences and* [b]*Department of Physics and Materials Science, The Ångström Laboratory, Uppsala University, SE-751 21 Uppsala, Sweden*
[c]*ChromoGenics AB, SE-75323 Uppsala, Sweden*
[d]*AGL Technologies S/A, LV-1007 Riga, Latvia*
[e]*Brazilian Synchrotron Light Laboratory, 13084-971 Campinas, Sao Paulo, Brazil*

Electrochromic (EC) films of nickel oxide, with and without vanadium, were prepared by reactive dc magnetron sputtering. They were characterized by electrochemical and optical measurements and studied by X-ray photoelectron spectroscopy (PES) using synchrotron radiation. The films were analyzed under as-deposited conditions and after bleaching/coloration by insertion/extraction of protons from a basic solution and ensuing charge stabilization. Optical measurements were consistent with a coloration process due to charge-transfer transitions from Ni^{2+} to Ni^{3+} states. The PES measurements showed a higher concentration of Ni^{3+} in the colored films. Moreover, two peaks were present in the O 1s spectra of the bleached film and pointed to contributions of $Ni(OH)_2$ and NiO. The changes in the O 1s spectra upon coloration treatment indicate the presence of Ni_2O_3 in the colored film and necessitated an extension of the conventional model for the mechanism of EC coloration. The model involves not only proton extraction from nickel hydroxide to form nickel oxyhydroxide but also participation of NiO in the coloration process to form Ni_2O_3.
 [DOI: 10.1149/1.3148327]

Manuscript submitted January 9, 2009; revised manuscript received May 12, 2009. Published June 12, 2009.

Electrochromic (EC) materials are able to change their optical properties reversibly and persistently upon charge insertion/extraction under the application of an external voltage.[1] Materials that color upon charge insertion/extraction are called cathodic/anodic. These materials can be implemented in energy-saving and comfort-enhancing architectural "smart windows," and other application areas include mirrors with variable specular reflectance, nonemissive information displays, surfaces with variable thermal emittance, eyewear, etc.[1-4] EC technology has been used for some niche applications for several years. However, the situation is now changing and electrochromism will reach wider applications.[5]

Thin films of Ni oxide possess anodic electrochromism, as discovered in the mid-1980s[6-9] and subsequently studied in a large number of investigations.[1-4] The visual appearance goes between transparent and brown upon extraction and insertion of charge. In EC devices incorporating cathodically coloring W oxide films, the brown color of Ni oxide is complementary to the blue color of W oxide, both together yielding a neutral (gray) color in transmittance for dark films.[4]

Ni oxide films produced for EC applications exhibit a cubic polycrystalline structure[1,9-14] and a density between 3 and 6.5 g/cm^3 depending on deposition conditions.[1,14,15] The low density is indicative of porosity.[10,14,16] The grain size depends strongly on film deposition conditions and can range from 3 to 300 nm.[9,10,12,14,15,17] The porosity and small grain size, leading to a large surface-to-bulk ratio, increase the EC activity of the films,[12,18,19] and the reaction that produces the color takes place in the outermost parts of the grains.[12]

Several varieties of reactively sputter-deposited EC hydrated nickel-based oxide thin films have been reported.[1-4,20] Optimized $Ni_{1-x}V_xO_y$ films made by sputter deposition exhibited a luminous transmittance as high as 74% when the deposition had been conducted in plasma of Ar + O_2 + H_2.[3,20] The addition of V facilitates magnetron sputtering but has little influence on the EC properties, as further discussed below.

Electrochromism in Ni oxide is surprisingly poorly understood despite the large amount of prior work and the technological importance of this material. We therefore initiated a concerted effort for which earlier results, focused on proton transport, were reported in a companion paper.[21] In particular, many reaction schemes have been proposed for charge insertion and extraction in hydrated Ni oxide thin films with EC properties. However, no concrete and convincing evidence for the reaction mechanism has been presented until now. Our previous work[21] pointed out the validity of the well-known Bode reaction scheme,[22,23] i.e.

$$\begin{array}{ccc} \beta - Ni(OH)_2 & \leftrightarrow & \beta - NiOOH \\ \updownarrow & & \updownarrow \\ \alpha - Ni(OH)_2 & \leftrightarrow & \gamma - NiOOH \end{array} \quad [1]$$

This model is elaborated and given further support below. Detailed studies of the coloration mechanism call for a surface-sensitive analysis method, and in particular X-ray photoelectron spectroscopy (PES), as employed in the present investigation, is a powerful tool.

Experimental

Film deposition.— EC Ni oxide-based thin films were deposited by reactive dc magnetron sputtering from 5 cm diameter targets of Ni and $NiV_{0.08}$ (purity 99.95%). The proportions of the gases in the plasma were approximately 96% Ar, 2% O_2, and 2% H_2 for sputtering of $Ni_{1-x}V_xO_y$ films and 79.2% Ar, 4.8% O_2, and 16% H_2 for sputtering of NiO_y. The total sputter pressure was 30 mTorr and the sputtering power was 200 W. The target-substrate distance was 13 cm. More details about the deposition were given elsewhere.[20]

The substrates used for optical and electrochemical measurements were glass plates precoated with a layer of indium tin oxide (ITO) (i.e., In_2O_3:Sn),[24,25] with a resistance/square of 60 Ω. Graphite substrates were employed for composition determinations using Rutherford backscattering spectrometry (RBS). Typical film thicknesses, recorded by surface profilometry across a masked edge, were 200 nm.

Physical techniques.— RBS was used to determine the elemental composition of the films[21] by analyzing the backscattered yield upon bombardment with 2.0 MeV α particles.

Spectrophotometric measurements were conducted on films that had been withdrawn from the electrolyte (see below) and cleaned in deionized water. Specifically, we measured normal transmittance T and near-normal reflectance R by use of a Perkin-Elmer double-beam spectrophotometer operating in the $300 < \lambda < 2500$ nm wavelength range, employing an integrating sphere. Barium sulfate served as a reference for the reflectance measurements.

* Electrochemical Society Active Member.
z E-mail: gunnar.niklasson@angstrom.uu.se

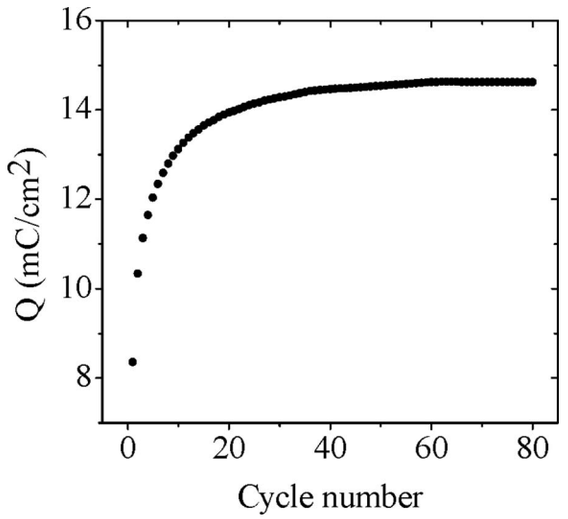

Figure 1. Evolution of charge capacity Q vs number of voltammetric cycles during charge stabilization of a hydrated $Ni_{1-x}V_xO_y$ film in 1 M KOH at a sweep rate of 10 mV/s.

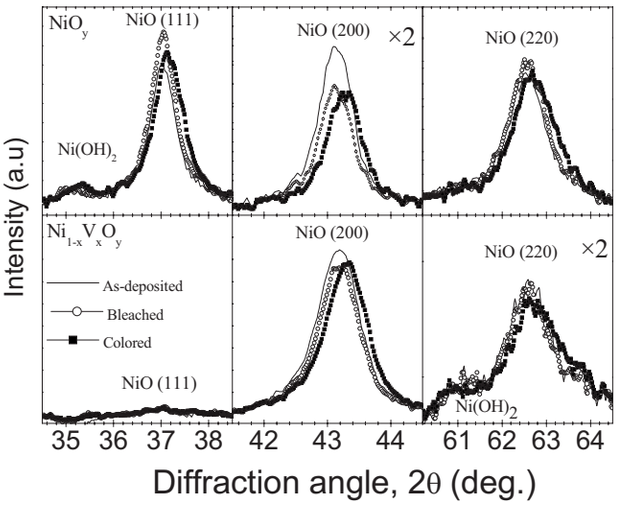

Figure 2. X-ray diffractograms of as-deposited and charge-stabilized films of NiO_y (upper panels) and $Ni_{1-x}V_xO_y$ (lower panels). Data are shown for as-deposited films (lines) and for stabilized films in colored (filled squares) and bleached states (circles). The assignment of the observed diffraction peaks for NiO as well as for some hydroxide features are shown.

Electrochemical techniques.— Cyclic voltammetry (CV) was carried out in a 1 M KOH electrolyte at a scan rate of 10 mV/s using a three-electrode configuration. A counter electrode of Pt and a reference electrode of Ag/AgCl (1 M KCl) were used. Typical data were obtained with a low (bleaching) potential of −0.65 V and a high (coloring) potential of +0.65 V. The experiment was carried out with an Autolab PGSTAT10 potentiostat.

Synchrotron facilities.— The photoelectron measurements were performed using synchrotron light (line BL I411) at the Swedish National Laboratory MAX in Lund.[26,27] The photoelectron take-off angle with respect to the sample surface plane was 70° and the angle between photon polarization and photoelectron direction was 0°.

X-ray diffraction (XRD) for structural analysis was performed at the Brazilian Synchrotron Light Laboratory (line D12A) using a 1.37 GeV storage ring. A photon energy of 8044 eV was used in a parallel-beam geometry.

Sample pretreatment.— The films were pretreated in 1 M KOH by CV after deposition and before physical measurements. To elucidate the evolution of the films, we prepared samples of three types for in-depth study: They were as deposited (type I), subjected to 5 CV cycles and colored or bleached (type II, referred to as non-charge-stabilized), and subjected to 70 CV cycles and colored or bleached (type III, referred to as charge-stabilized). After cycling, the films were rinsed in distilled water, dried with nitrogen, and put into the vacuum chamber for XRD and X-ray photoelectron spectroscopy (XPS) analyses. As will become apparent later, the pretreatment led to hydroxylation of the films.

Quantitative data on charge capacity Q were determined from CV data; they were recorded after cathodic bleaching to avoid possible contributions due to oxygen production. Figure 1 shows the evolution of Q during cycling. Specifically, Q grew from an initial value of ~8 mC/cm^2 to a stabilized value of ~15 mC/cm^2 after 70 cycles. Similar changes were reported several times in the past.[1]

Sample Characterization

Composition and density.— The film composition was found by RBS to correspond to O/Ni = 1.51 and V/Ni = 0.09 for $Ni_{1-x}V_xO_y$ samples with optimum EC properties. For NiO_y films, prepared under similar conditions, the O/Ni ratio was approximately 1.3.[28] The density was ~4.0 g/cm^3 for both types of film, i.e., much below 6.67 g/cm^3 applying to stoichiometric NiO. Judging from the literature, we expect these films to exhibit high porosity and small grain size.[10]

Structural analysis.— Figure 2 illustrates XRD spectra for three selected angle intervals within the $35 < 2\theta < 65°$ range for as-deposited and stabilized films of NiO_y (upper panels) and $Ni_{1-x}V_xO_y$ (lower panels). The diffraction peaks of cubic nickel oxide (bunsenite)[29] are labeled, as well as some features attributed to hydroxide phases.[29] The ITO contribution was eliminated by dividing the total spectrum with the normalized spectrum for an ITO/glass sample prepared under analogous conditions. Some differences in the diffraction features are observed between NiO_y and $Ni_{1-x}V_xO_y$. Distinct (111), (200), and (220) peaks due to NiO are seen in the NiO_y spectrum as well as weak reflections originating from the highly hydrated phases of nickel hydroxide and oxyhydroxide. However, for the $Ni_{1-x}V_xO_y$ film, the (111) reflections are not manifested (cf. lower left-hand panel in Fig. 2), pointing to the presence of a strong texture. Peak positions of the hydroxides and oxyhydroxides can vary due to the different contents of structural water of the compounds and the morphology of the nanostructures that will affect the degree of disorder present in the different phases. Additional weak features related to $Ni(OH)_2$ may be inferred from the asymmetric shape of the NiO peaks.

Several minor changes in the diffraction spectra between the as-deposited, bleached, and colored states of the films are apparent in Fig. 2. These are however difficult to interpret in detail. The observed shift toward larger diffraction angles upon coloration may be associated with stress, which is known to develop in conjunction with ion intercalation.[30] The data give clear evidence for the presence of the hydroxide phases. The stabilized oxyhydroxide phase is produced solely via hydrogen transport, as shown before.[21]

No separate phases associated with V were detected, which agrees with our earlier work[31] in which extended X-ray absorption fine-structure analysis on films similar to the present ones showed that the V atoms substituted nickel in a NiO-type structure, i.e., Ni and V appeared to form a mixed-oxide phase in the film.

Optical characterization.— T and R were recorded as a function of wavelength for as-deposited and for charge-stabilized colored and bleached films for the latter cases at maximum optical contrast, i.e., when the current density approached zero during CV measurements.

Optical spectra were Ni-oxide-like and resembled literature data.[1,4,21] Absorption coefficient a was obtained from the expression[32]

$$a(\lambda) = d^{-1} \ln\{[1 - R(\lambda)]/T(\lambda)\} \quad [2]$$

where d is the film thickness. This approximation holds well when the refractive index of the substrate is between 1.5 and 1.7 and the refractive index of the coating is between 1.3 and 2.5; the formula gives a relative error of around 10% and a maximum relative error less than 15% for a high refractive-index coating.

Figure 3a shows data on a for charge-stabilized bleached and colored hydrated NiO_y and $Ni_{1-x}V_xO_y$ films. The absorption above 3.5 eV is largely due to the ITO base layer and the glass substrate. The spectrum for the bleached films did not exhibit any structure in the studied energy range. Plotting ln α vs photon energy, a linear dependence could be observed between 3.5 and 3 eV. This behavior is referred to as an "Urbach tail" and may be related to excitations between localized states in the bandgap and the band edges.[33,34] Figure 3b shows the difference between the absorption spectra of the colored and bleached states. A broad peak with a maximum around 3 eV can be seen for both films.

Figure 3c shows numerically calculated derivatives with respect to energy of both spectra. Overlapping peaks in absorption spectra can often be resolved in derivative spectra, and a peak in the absorption coefficient then corresponds to a decreasing step in the first derivative.[35] The spectra in Fig. 3c display two such structures in the measured energy range, namely, at 2.1 ± 0.2 and 2.8 ± 0.2 eV. They are clearly seen in the $Ni_{1-x}V_xO_y$ spectrum but also upon close scrutiny in the NiO_y spectrum.

We now compare the absorption peaks in Fig. 3c to previous results on optical absorption features. Data on as-deposited films, made by sputtering in an excess of O_2, showed peaks at 1.1 and 1.7 eV.[36] They lie close to peaks observed at 1.1 and 1.8 eV in oxidized Ni.[37] These spectra have been rationalized within semiempirical molecular-orbital theory for charge-transfer excitations in $NiO{\cdot}Ni_2O_3$. We tentatively assign our peak at 2.1 eV to the higher of these transitions, but we were not able to resolve any features in our spectra at lower energies.

The other peak, at around 2.8 eV, is consistent with the optical absorption in NiOOH. Unfortunately optical data on this oxyhydroxide are scarce. Results on electrochemically oxidized NiOOH, with uncertain crystallinity and purity, displayed a broad absorption peak at 2.7–2.8 eV.[38] This absorption was due to strong crystal-field effects.[39]

Summarizing the discussion around Fig. 3, we suggest that the absorption features in the colored films are consequences of the presence of two compounds wherein the Ni ion is in valence state 3+, viz., NiOOH and Ni_2O_3.

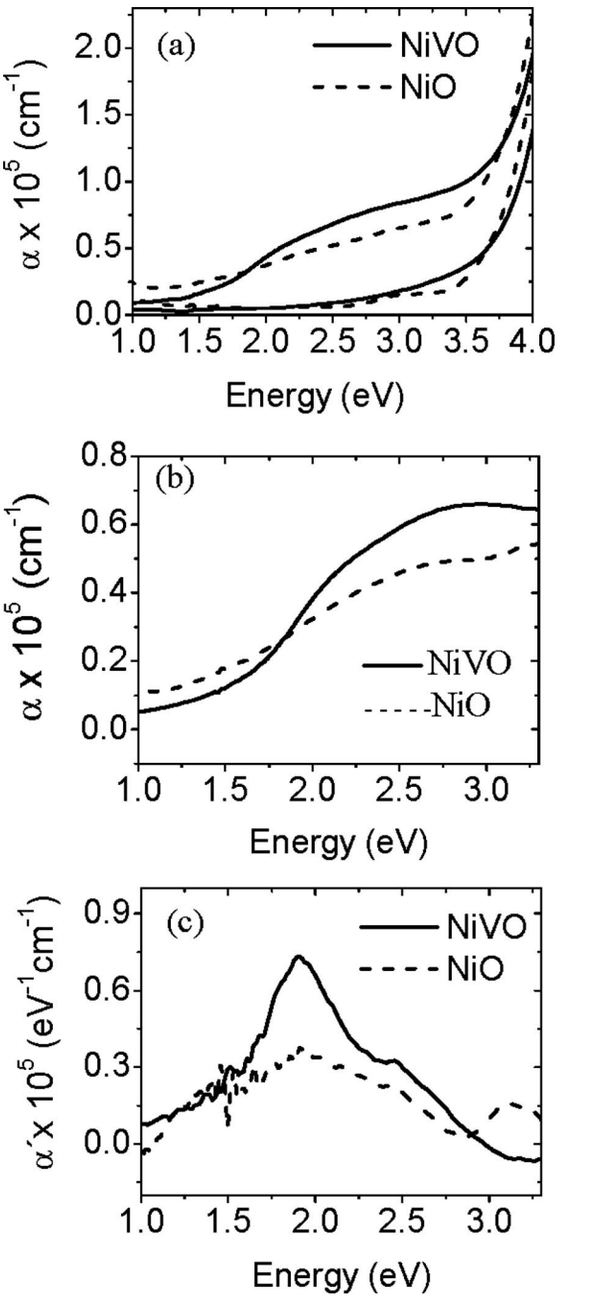

Figure 3. (a) Absorption coefficient α vs photon energy at visible and near-IR wavelengths for charge-stabilized colored (upper two curves) and bleached (lower curves) NiO_y and $Ni_{1-x}V_xO_y$ films, (b) the difference between the absorption coefficients of the colored and bleached states for NiO_y and $Ni_{1-x}V_xO_y$ films, and (c) the derivative of the absorption coefficient curves in (b) (denoted α′).

PES Data

General.— In this section we concentrate on $Ni_{1-x}V_xO_y$ films. PES measurements were made on core states of Ni, O, and V and on the states forming the top of the valence band. Data are given in Fig. 4-9. The measured spectra were normalized with respect to the area of the Ni 2p core states, and the binding energy (BE) calibration was done by placing the BE of the adventitious carbon at 285 eV.[40]

The Ni 2p spectra for oxides are complex, and the literature contains a set of different interpretations. Generally the Ni $2p_{3/2}$ states in NiO give rise to multiple peaks at BEs between 852 and 860 eV.[41-44] For example, for a well-crystallized NiO sample two peaks centered at ~854.6 and ~856.1 eV are observed, and the ratio between the lower BE peak and the higher BE peak is considerably above unity.[44] A nonperfect nickel oxide contains excess oxygen, and for each extra oxygen atom (nickel vacancy) there are two Ni atoms in the 3+ oxidation state. These states contribute with a feature centered at ~855.7 eV, i.e., at a position between the two peaks pertaining to NiO. The Ni $2p_{3/2}$ peak in $Ni(OH)_2$ may also contribute in this range.[44] In a measured PES signal, the contribution of the 3+ states will cause the double peak to appear with an altered intensity ratio, and simple curve-fitting analysis for quantitative predictions is difficult. The following discussion is therefore mainly based on qualitative assessments involving comparison to model compounds such as those reported elsewhere.[44]

The O 1s states in oxide phases of NiO and Ni_2O_3 give a single peak centered at ~529.7 [45,46] and ~531.7 eV,[45] respectively. In the hydroxide-containing phases $Ni(OH)_2$ and NiOOH, the situation is not so clear and peak values between ~530.5 and ~531.7 eV have been obtained.[42,45,47-49] Furthermore, NiOOH can hardly be distin-

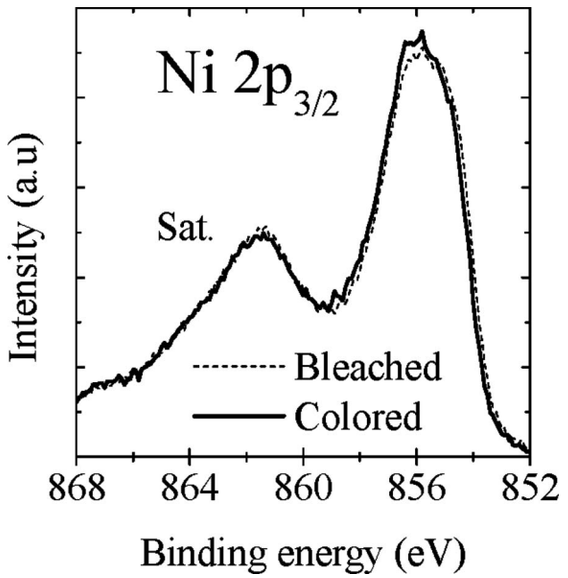

Figure 4. PES spectra for Ni 2p core states of charge-stabilized $Ni_{1-x}V_xO_y$ films under colored and bleached conditions. A satellite (sat), due to final-state effects, is seen. The vertical scale gives intensity in arbitrary units (a.u.). A photon energy of 1061 eV was used.

guished from hydrated forms of Ni_2O_3.[49,50] The O 1s peak emanating from adsorbed H_2O or OH^- groups is centered at ~532.7 eV.[51] In practice all of these peaks overlap, and the intensity redistribution within the measured spectral feature can be used to give evidence for possible phase transformations taking place during charge stabilization in the beginning of the electrochemical cycling (cf. Fig. 1) and upon coloration and bleaching.

Nickel $2p_{3/2}$ core states.— Figure 4 shows PES spectra for Ni $2p_{3/2}$ states in a charge-stabilized $Ni_{1-x}V_xO_y$ film in bleached and colored states. The structure of both spectra is similar to that previously found for NiOOH [44] and therefore points at a large presence of Ni^{3+} states under both conditions, i.e., no clear contribution from NiO in the surface region is observed.

Figure 5 reports spectra pertinent to Ni $2p_{3/2}$ states of non-charge-stabilized $Ni_{1-x}V_xO_y$ films under as-deposited, colored, and bleached conditions. Again the areas under the curves are very similar. Compared to the structures discussed above, the spectrum from the as-deposited films indicates the presence of NiO in the surface region. The similarity of the spectra of as-deposited and bleached films suggests that there is a comparable mixing in these films. Similar to the case of charge-stabilized films, a spectrum resembling that of NiOOH is observed for the colored non-charge-stabilized films.

Oxygen 1s core states.— Figure 6 shows O 1s states for charge-stabilized $Ni_{1-x}V_xO_y$ films under colored and bleached conditions measured at two photon energies. Having in mind the optical data and the XRD spectra reported previously for different phases of nickel oxides and hydroxides, the increase in the peak at lower BE in the spectrum of the bleached film is consistent with an increase in the amount of NiO. The spectrum of the colored film has an additional contribution in the energy interval expected from a hydrated phase. In PES, the surface sensitivity depends on the kinetic energy of the emitted electrons so that the measurements become increasingly more surface sensitive at lower kinetic energies (lower photon energies). From the photon energy dependence, Fig. 6, the hydrated phases dominate at the surface, as expected, while more NiO is in the bulk.

Figure 7 shows spectra for O 1s states for non-charge-stabilized $Ni_{1-x}V_xO_y$ films under as-deposited, colored, and bleached conditions. The peak at ~529.7 eV is reduced in intensity upon going from as-deposited, to bleached, and then to colored conditions. In line with the discussion above, this change can be attributed to a transformation of the Ni oxide to hydroxide during initial cycling. These spectra also support the results from the Ni 2p spectra of the nonstabilized samples discussed above and indicate that the amounts of NiO in the surface layers are much higher in the nonstabilized films. The transformation of Ni oxide to hydroxide may involve excess oxygen, present in the films from the beginning, together with protons and hydroxyl groups introduced during CV cycling and electrons supplied from or extracted into the outer circuit. The charge inserted into and extracted from the film is not exactly balanced during the first cycles.

The O/Ni ratio at the surface was calculated by subtraction of the XPS background and subsequent integration of the spectra for the Ni

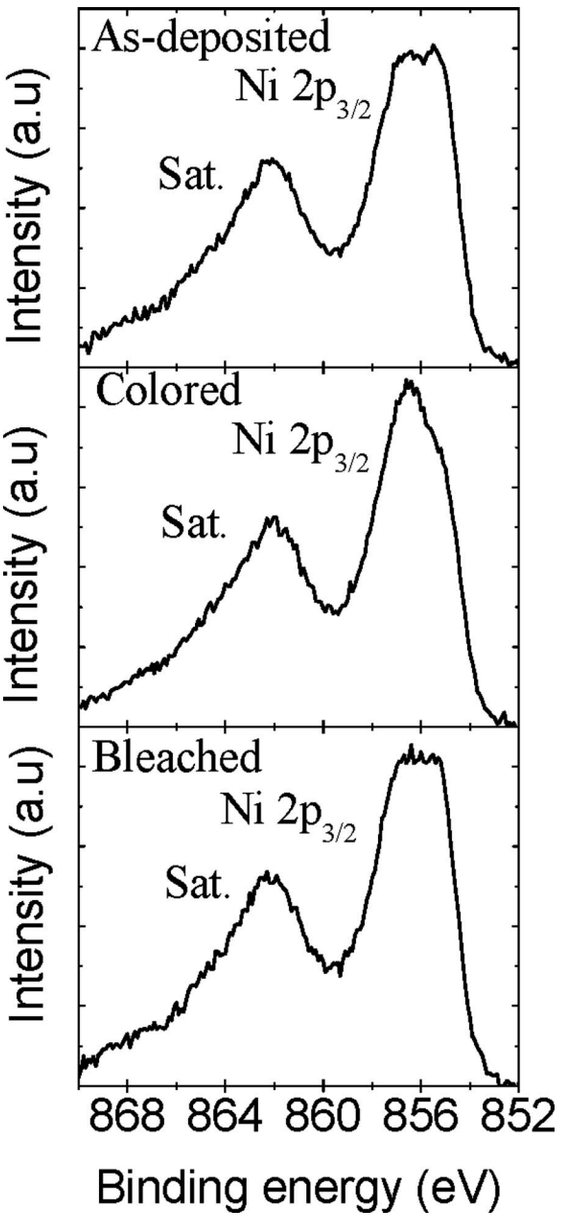

Figure 5. PES spectra for Ni 2p core states of non-charge-stabilized $Ni_{1-x}V_xO_y$ films in as-deposited, colored, and bleached conditions. A satellite (sat), due to final-state effects, is seen. The vertical scale gives intensity in arbitrary units. A photon energy of 1250 eV was used.

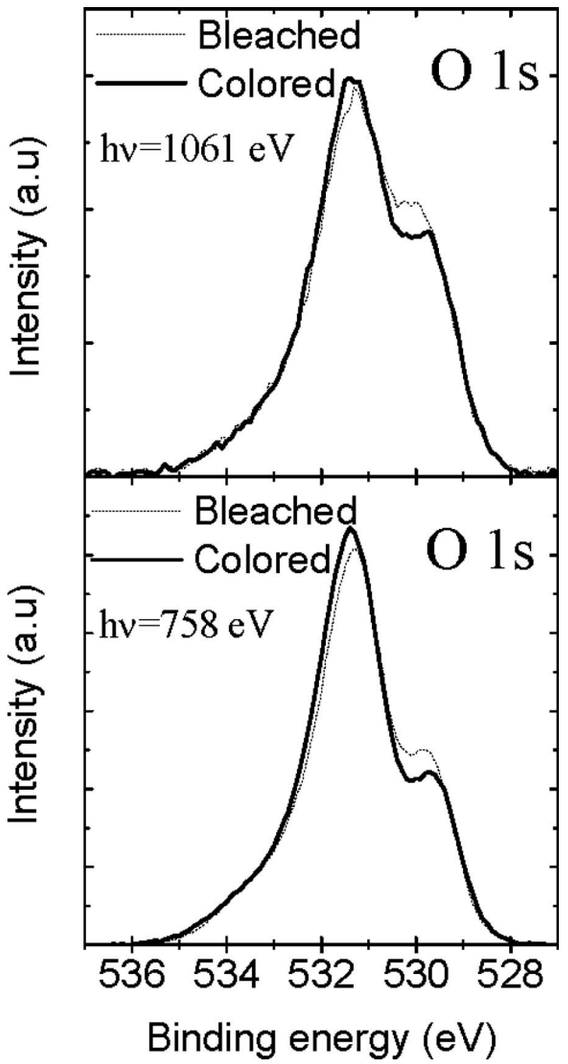

Figure 6. PES spectra for O 1s core states of charge-stabilized $Ni_{1-x}V_xO_y$ films in colored and bleached conditions. The vertical scale gives intensity in arbitrary units. Photon energies *hν* of 1061 and 758 eV were used.

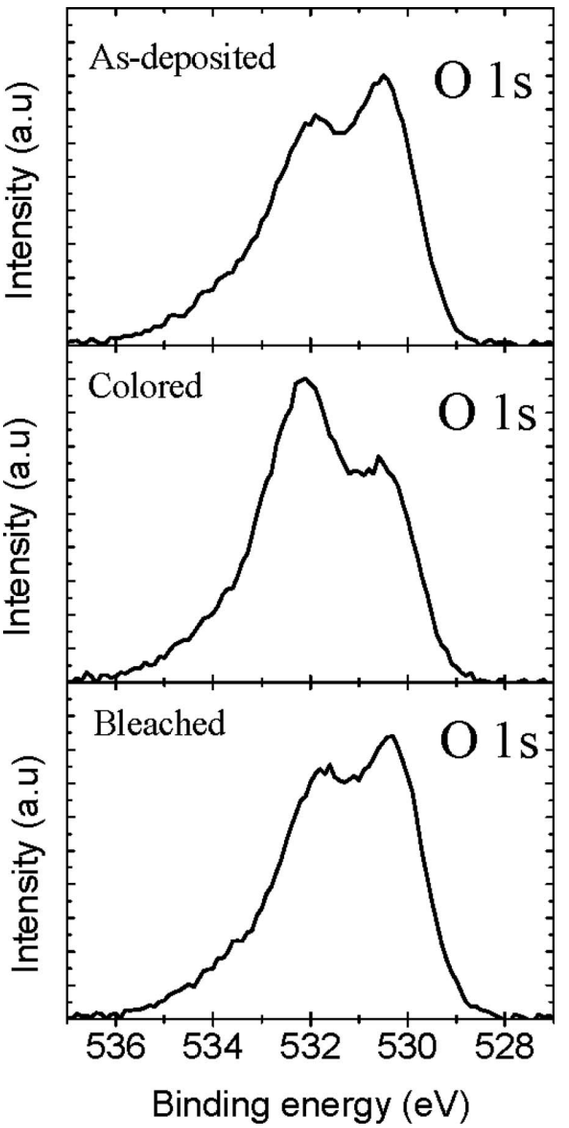

Figure 7. PES spectra for O 1s core states of non-charge-stabilized $Ni_{1-x}V_xO_y$ films in as-deposited, colored, and bleached conditions. The vertical scale gives intensity in arbitrary units. A photon energy of 1250 eV was used.

2p states divided by corresponding values obtained for the O 1s states. The O/Ni ratio for non-charge-stabilized films increased from the as-deposited to the bleached state by approximately 7%, and further from the bleached to the colored state by approximately 2%. This may be caused by OH^- uptake during charge stabilization. For the charge-stabilized films, the difference between the O/Ni ratio for the bleached and colored conditions was less than 1%, thus proving that there was no significant transport of oxygen upon cycling. The fact that the O/Ni ratio remains practically unchanged is important because it disproves the existence of interchange of hydroxyl groups and points at intercalation of protons during coloration after the charge has been stabilized. Additional evidence for the overriding role of protons was obtained from work on Pd-coated $Ni_{1-x}V_xO_y$ films in earlier work.[21]

Vanadium 2p core states.— Figure 8 shows spectra for V 2p states for non-charge-stabilized $Ni_{1-x}V_xO_y$ films under as-deposited, colored, and bleached conditions. Corresponding spectra for the charge-stabilized films were very similar. The V 2p states did not show any BE shift under coloration, meaning that no valence change was induced upon CV cycling. V is not electrochemically active upon coloration. The relative change in the area of V/Ni between as-deposited and bleached states was negligible; in the colored state the relative area decreased by ~30%. A possible explanation for these features is that vanadium always stays in the NiO phase and that the decrease indicates the formation of a vanadium-free colored surface layer.

Valence-band states.— Figure 9 shows the top of the valence band for charge-stabilized $Ni_{1-x}V_xO_y$ films in colored and bleached states. A change in intensity of the spectrum is observed, indicating a depopulation of electrons in the colored state with respect to the bleached state.

Discussion

The mechanisms of EC coloration in NiO_y and $Ni_{1-x}V_xO_y$ films upon electrochemical cycling are discussed next. Based on the structural, optical, and electrochemical measurements, the coloration was due to the base material (i.e., nickel oxide) even in the films with some vanadium. Thus the role of the V is only to influence the bleached state transmittance of the films, and V shows neither opti-

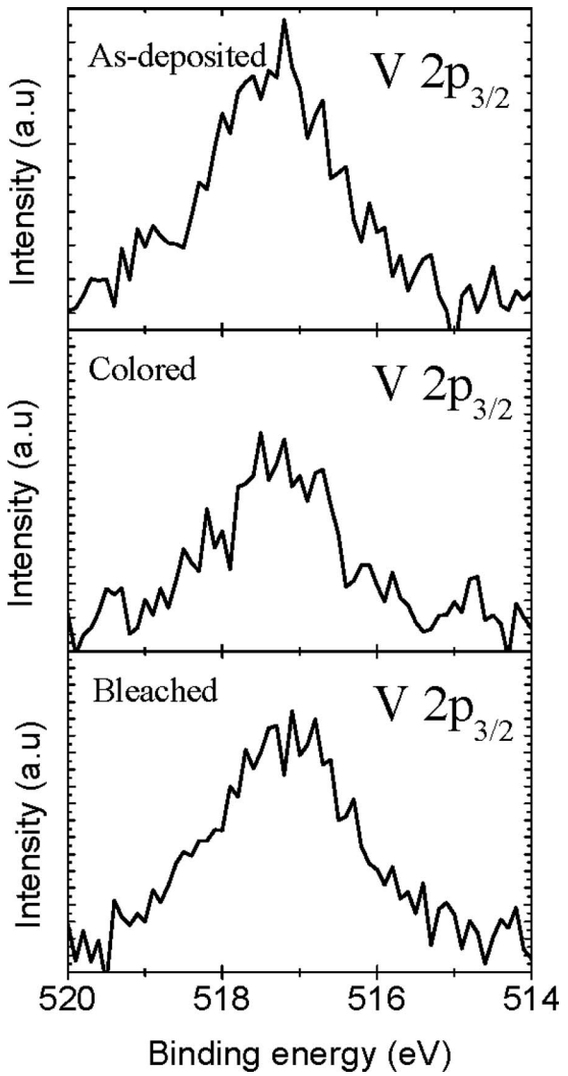

Figure 8. PES spectra for V 2p core states of non-charge-stabilized $Ni_{1-x}V_xO_y$ films in as-deposited, colored, and bleached conditions. The vertical scale gives intensity in arbitrary units. A photon energy of 1250 eV was used.

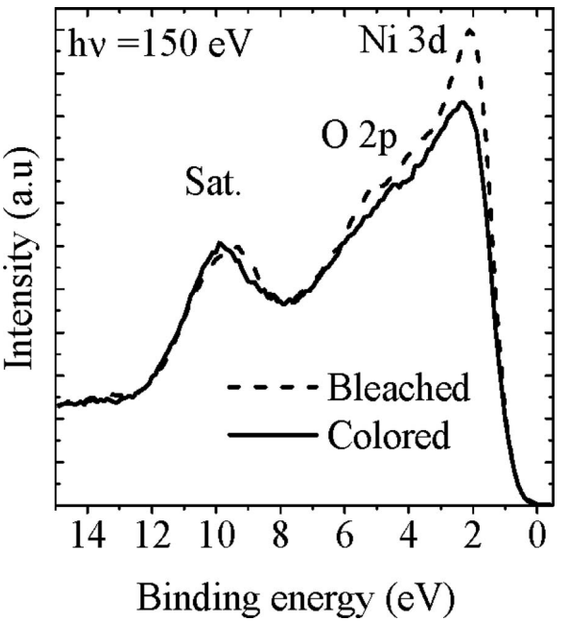

Figure 9. PES spectra for Ni 3d and O 2p valence states of charge-stabilized $Ni_{1-x}V_xO_y$ films in colored and bleached conditions. The V 3d and Ni 3d states overlap. A satellite (sat.), due to final-state effects, is seen. The vertical scale gives intensity in arbitrary units (a.u.). A photon energy of 150 eV was used. The spectra were normalized with respect to the background.

cal nor electrochemical activity during charge insertion. The fact that V was present in the films will be disregarded in the discussion below.

There is an excess of oxygen in the as-deposited films, which are characterized by low density (high porosity) and small grain size. The PES data show that the outermost parts of the grains are richer in hydroxide and oxyhydroxide phases than the bulk. Independent of the color condition, there are always Ni atoms in valence states 2+ and 3+. From optical and PES spectra the number of nickel sites with 3+ state is increased upon coloration.

The NiO and corresponding hydroxide structures were detected by XRD. The XRD spectra show the presence of bulk NiO both initially and in the colored and bleached charge-stabilized states. The surface-sensitive PES spectra also show that some NiO is transformed to hydroxide and oxyhydroxide during stabilization. This transformation takes place at the electrolyte/film interface. This also indicates that the coloration process is a surface phenomenon, most likely in the outer parts of the grains, rather than a bulk change. This hypothesis also correlates with the fact that the EC activity increases when the inner surface area is increased by the decrease in the grain size.[12,18,19]

In the beginning of the electrochemical treatment, several cycles are required for the charge capacity to reach its maximum value and stabilize (Fig. 1), and changes in the film structure and composition can be observed during the stabilization. PES results are consistent with a transformation of overstoichiometric-hydrated Ni oxide to hydroxide and oxyhydroxide phases on the grain surfaces. The amount of oxygen in the films increases slightly by intercalation of OH^- groups during stabilization. Our previous results,[21] based on the galvanostatic intermittent titration technique, suggested crystallization of the hydroxide and oxyhydroxide phases during the initial CV cycles.

The coloration mechanism in charge-stabilized films was studied in detail by PES. Excess oxygen in NiO produces Ni^{2+} vacancies which are compensated by creation of holes on two Ni^{2+} sites, thereby producing Ni^{3+}.[52] To account for our PES results, a process that is additional to the well-known Bode reaction, stated in the introduction, can be suggested.[22,23] It involves proton extraction from $Ni(OH)_2$ as well as a valence change in nickel atoms belonging to the NiO phase. The extraction of H^+ causes a transformation from $Ni(OH)_2$ to NiOOH, and the extraction of another H^+ is compensated by creation of a hole on the Ni^{2+} belonging to the NiO unit. This process results in the formation of Ni_2O_3.

The surface sensitivity is a few atomic layers for the Ni 2p and O 1s core levels at a photon energy of 1061 eV. Because the coloration is a surface effect and the bulk remains NiO independent of whether the film is bleached or colored, one can argue that after the transformation of the $Ni(OH)_2$ to NiOOH the change in the NiO to Ni_2O_3 may be in the interface between the NiO and the nickel oxyhydroxide. Such an interphase forms a bridge between the cubic NiO and the hexagonal phases of $Ni(OH)_2$ and NiOOH. This may explain the shift of the NiO (200) diffraction peak in Fig. 2 for the colored state because the contraction on the outermost part of the grains produces an increase in the strain in the inner part.

The top of the valence band, as apparent from Fig. 9, showed a

decrease in intensity upon coloration. A depopulation of the electronic states in the upper part of the valence band is also indicative of a valence change from 2+ to 3+ upon coloration.

Conclusion

Thin films of hydrated nickel vanadium oxide were deposited by reactive dc magnetron sputtering in a gas mixture of $Ar + O_2 + H_2$. The films showed excellent electrochromism even from the first voltammetric cycles. The only noticeable influence of vanadium was a slight lowering of the bleached state transmittance. An increase in the charge capacity upon initial voltammetric cycling occurs together with a transformation of the nickel oxide into nickel hydroxide at grain boundaries, while the bulk of the grains remains cubic nickel oxide, as detected by XRD and PES.

Changes in the O 1s core levels, probed by PES, indicate that it is necessary to extend the Bode reaction mechanism for the coloration. The O 1s states show a decrease in the oxygen bonded to Ni in nickel oxide and a shift and increase in the oxygen bonded to the hydroxide and oxyhydroxide phases. Because coloration is due to extraction of protons, we propose a mechanism analogous to the one for the oxidation of nickel monoxide to dinickel trioxide through the creation of Ni^{2+} vacancies. The dehydrogenation of the nickel oxyhydroxide leaves a vacancy that is compensated by the creation of a hole in the nickel monoxide.

Hence, based on XRD, PES, as well as proton diffusion analyses reported before,[21] the coloration mechanism for EC nickel oxide can be written as

$$\begin{aligned} &\beta - \mathrm{Ni(OH)_{2\ bleached}} \\ &\updownarrow \\ &\alpha - \mathrm{Ni(OH)_{2\ bleached}} \leftrightarrow \gamma - \mathrm{NiOOH_{\ colored}} + \mathrm{H^+} + \mathrm{e^-} \\ &\mathrm{NiO} + \alpha - \mathrm{Ni(OH)_{2\ bleached}} \leftrightarrow \mathrm{Ni_2O_{3\ colored}} + 2\mathrm{H^+} + 2\mathrm{e^-} \end{aligned} \quad [3]$$

which clearly is an extension of the Bode reaction scheme shown in Reaction 1 in the introduction.

Acknowledgments

This work was supported by a grant from the Swedish Research Council (VR). E.A. is grateful for a scholarship received from the University of Costa Rica to complete his Ph.D. at Uppsala University. The Maxlab (Sweden) and LNLS (Brazil) synchrotron light sources are acknowledged for their technical support and assigned beam time. We are grateful to Jens Jensen and Göran Possnert at Uppsala University for assistance with RBS measurements and to Sara Green for useful discussions.

Uppsala University assisted in meeting the publication costs of this article.

References

1. C. G. Granqvist, *Handbook of Inorganic Electrochromic Materials*, Elsevier, Amsterdam (1995) (reprinted 2002).
2. C. G. Granqvist, *Sol. Energy Mater. Sol. Cells*, **60**, 201 (2000).
3. C. G. Granqvist, E. Avendaño, and A. Azens, *Thin Solid Films*, **442**, 201 (2003).
4. G. A. Niklasson and C. G. Granqvist, *J. Mater. Chem.*, **17**, 127 (2007).
5. C. G. Granqvist, *Nature Mater.*, **5**, 89 (2006).
6. J. S. E. M. Svensson and C. G. Granqvist, *Appl. Phys. Lett.*, **49**, 1566 (1986).
7. J. S. E. M. Svensson and C. G. Granqvist, *Appl. Opt.*, **26**, 1554 (1987).
8. J. S. E. M. Svensson and C. G. Granqvist, *Sol. Energy Mater.*, **16**, 19 (1987).
9. W. Estrada, A. M. Andersson, and C. G. Granqvist, *J. Appl. Phys.*, **64**, 3678 (1988).
10. D. A. Wruck and M. Rubin, *J. Electrochem. Soc.*, **140**, 1097 (1993).
11. M. Kitao, K. Izawa, K. Urabe, T. Komatsu, S. Kuwano, and S. Yamada, *Jpn. J. Appl. Phys., Part 1*, **33**, 6656 (1994).
12. E. L. Miller and K. E. Rocheleau, *J. Electrochem. Soc.*, **144**, 1995 (1997).
13. K. Yoshimura, T. Miki, and S. Tanemura, *Jpn. J. Appl. Phys., Part 1*, **34**, 2440 (1995).
14. I. C. Faria, M. Kleinke, A. Gorenstein, M. C. A. Fantini, and M. H. Tabacniks, *J. Electrochem. Soc.*, **145**, 235 (1998).
15. G. Bajars, Y. A. Pitkevich, A. Lusis, É. V. Pentyush, J. Benders, and V. Bets, *Elektrokhimiya*, **25**, 336 (1989) [*Sov. Electrochem.*, **25**, 749 (1989)].
16. W. Wagner, F. Rauch, and K. Bange, *Nucl. Instrum. Methods Phys. Res. B*, **89**, 104 (1994).
17. K. Yoshimura, T. Miki, and S. Tanemura, *Mater. Res. Bull.*, **32**, 839 (1997).
18. M. K. Carpenter, R. S. Conell, and D. A. Corrigan, *Sol. Energy Mater.*, **16**, 333 (1987).
19. A. Azens, L. Kullman, G. Vaivars, H. Nordborg, and C. G. Granqvist, *Solid State Ionics*, **113–115**, 449 (1998).
20. E. Avendaño, A. Azens, J. Isidorsson, R. Karmhag, G. A. Niklasson, and C. G. Granqvist, *Solid State Ionics*, **165**, 169 (2003).
21. E. Avendaño, A. Azens, G. A. Niklasson, and C. G. Granqvist, *J. Electrochem. Soc.*, **152**, F203 (2005).
22. H. Bode, K. Dehmelt, and J. Witte, *Electrochim. Acta*, **11**, 1079 (1966).
23. H. Bode, K. Dehmelt, and J. Witte, *Z. Anorg. Allg. Chem.*, **366**, 1 (1969).
24. C. G. Granqvist and A. Hultåker, *Thin Solid Films*, **411**, 1 (2002).
25. C. G. Granqvist, *Sol. Energy Mater. Sol. Cells*, **91**, 1529 (2007).
26. S. Svensson, J.-O. Forsell, H. Siegbahn, A. Ausmees, G. Bray, S. Södergren, S. Sundin, S. J. Osborne, S. Aksela, E. Nömmiste, et al., *Rev. Sci. Instrum.*, **67**, 2149 (1996).
27. M. Bässler, J-.O. Forsell, O. Björneholm, R. Feifel, M. Jurvansuu, S. Aksela, S. Sundin, S. L. Sorensen, R. Nyholm, A. Ausmees, et al., *J. Electron Spectrosc. Relat. Phenom.*, **101–103**, 953 (1999).
28. S. Green, J. Backholm, P. Georen, C. G. Granqvist, and G. A. Niklasson, *Sol. Energy Mater. Sol. Cells*, doi: 10.1016/j.solmat.2009.05.009 (2009).
29. JDES diffraction files, NiO: PDF no. 04-003-5840; $Ni(OH)_2$: PDF no. 742075, no. 270956, and no. 401179.
30. J. Scarminio, W. Estrada, A. Andersson, A. Gorenstein, and F. Decker, *J. Electrochem. Soc.*, **139**, 1236 (1992).
31. E. Avendaño, A. Kuzmin, J. Purans, A. Azens, G. A. Niklasson, and C. G. Granqvist, *Phys. Scr., T*, **115**, 464 (2005).
32. W. Q. Hong, *J. Phys. D*, **22**, 1384 (1989).
33. F. Urbach, *Phys. Rev.*, **92**, 1324 (1953).
34. F. Moser and F. Urbach, *Phys. Rev.*, **102**, 1519 (1956).
35. M. Cardona, *Modulation Spectroscopy*, Solid State Phys. Suppl. 11, p. 105, Academic, New York (1969).
36. K. M. E. Miedzinska, B. R. Hollebone, and J. G. Cook, *J. Phys. Chem. Solids*, **49**, 1355 (1988).
37. F. J. Morin, *Phys. Rev.*, **93**, 1199 (1954).
38. R. W. Crocker and R. H. Muller, Lawrence Berkeley National Laboratory Report no. LBL-32136, University of California Berkeley, Berkeley, CA (1992); L. M. M. de Souza, F. P. Kong, F. R. McLarnon, and R. H. Muller, *Electrochim. Acta*, **42**, 1253 (1997).
39. M. Lo Jacono, A. Sgamellotti, and A. Cimino, *Z. Phys. Chem., Neue Folge*, **70**, 179 (1970).
40. J. F. Moulder, W. F. Stickle, P. E. Sobol, and K. D. Momben, *Handbook of X-Ray Photoelectron Spectroscopy*, Physical Electronics Inc., Eden Prairie, MN (1995).
41. S. Uhlenbrock, C. Scharfschwerdt, M. Neumann, G. Illing, and H.-J. Freund, *J. Phys.: Condens. Matter*, **4**, 7973 (1992).
42. N. S. McIntyre, T. E. Rummery, M. G. Cook, and D. Owen, *J. Electrochem. Soc.*, **123**, 1164 (1976).
43. J.-K. Kang and S.-W. Rhee, *Thin Solid Films*, **391**, 57 (2001).
44. A. P. Grosvenor, M. C. Biesinger, R. St. C. Smart, and N. S. McIntyre, *Surf. Sci.*, **600**, 1771 (2006).
45. K. S. Kim and N. Winograd, *Surf. Sci.*, **43**, 625 (1974).
46. A. N. Mansour, *Surf. Sci. Spectra*, **3**, 231 (1994).
47. A. N. Mansour and C. A. Melendres, *Surf. Sci. Spectra*, **3**, 271 (1994).
48. A. N. Mansour and C. A. Melendres, *Surf. Sci. Spectra*, **3**, 255 (1994).
49. L. M. Moroney, R. St. C. Smart, and M. W. Roberts, *J. Chem. Soc., Faraday Trans., 1*, **79**, 1769 (1983).
50. A. N. Mansour and C. A. Melendres, *Surf. Sci. Spectra*, **3**, 263 (1994).
51. M. Schulze, R. Reissner, M. Lorenz, U. Radke, and W. Schnurnberger, *Electrochim. Acta*, **44**, 3969 (1999).
52. P. A. Cox, *The Electronic Structure and Chemistry of Solids*, Oxford University, Oxford (1998).